Journal of Alloys and Compounds 898 (2022) 162946

Contents lists available at ScienceDirect

Journal of Alloys and Compounds

journal homepage: www.elsevier.com/locate/jalcom

The effect of graphene on structure and optical properties of CdSe nanoparticles for optoelectronic application

Ahmed I. Abdel-Salam[a,1], M.M. Awad[b,1], T.S. Soliman[c,d,*], A. Khalid[e]

[a] Nanotechnology Research Center (NTRC), British University in Egypt (BUE), El Shorouk City, Egypt
[b] Physics Department, Loughborough University, Loughborough, Leicestershire LE11 3TU, UK
[c] Physics Department, Faculty of Science, Benha University, Benha 13518, Egypt
[d] Institute of Natural Sciences and Mathematics, Ural Federal University, Ekaterinburg 620000, Russia
[e] Department of Basic Engineering Sciences, Faculty of Engineering (Shoubra), Benha University, Benha, Egypt

ARTICLE INFO

Article history:
Received 7 September 2021
Received in revised form 20 November 2021
Accepted 23 November 2021
Available online 27 November 2021

Keywords:
CdSe-rGO Nanocomposite
CdSe QDs
Optical parameters
Effective Mass Approximation
Polynomial Fitting Functions
Refractive index

ABSTRACT

CdSe-reduced Graphene Oxide (CdSe-rGO) nanocomposite was synthesized using a facile hot injection method with excellent control over the size and morphology. The superb distribution of the CdSe quantum dots (CdSe QDs) and the tightly anchoring to the graphene sheets enhance their optical properties. Therefore, the effect of reduced Graphene oxide (rGO) on the structure and optical properties of CdSe nanoparticles is studied by X-ray diffraction (XRD), UV–visible spectroscopy, and transmission electron microscopy (TEM). As well as Effective mass approximation model (EMA) and Polynomial Fitting Functions (PFF) were used to calculate the sizes of nanoparticles, yielding particle sizes ranging from 4.64 to 5.46 nm and 2.74–3.72 nm, respectively. These values were comparable to those obtained by TEM and XRD. Furthermore, the data revealed that the direct energy gap of the CdSe QDs was reduced from 2.33 eV for the smallest size to 2.17 eV for the largest size. The optical parameters of CdSe-rGO nanocomposite such as the refractive index and extinction coefficient were increased with the particle size growth. As well, optical dielectric constant and optical conductivity were improved due to the increase of the particle size of CdSe QDs in the CdSe-rGO nanocomposite. So, the capability of CdSe-rGO nanocomposite to tune the optical parameters makes it a suitable candidate for a wide range of applications, specifically optoelectronics.

1. Introduction

Carbon-based materials, particularly graphene, that is also considered as a distinct form of 2D material due to the presence of a flat single sheet of sp2 hybridized carbon atoms which densely packed into some kind of 2D honeycomb crystal lattice [1,2]. Graphene has raised the scientific community's interest due to its exceptional properties such as higher electrical, thermal, mechanical features, in addition to, its high surface area and complex surface characteristics [3–5]. Graphene is classified as a semiconductor with a zero band gap, which restricts its exploit in optoelectronics and photonics [6]. Various nanoparticles have been successfully deposited onto graphene sheets to extend the application range and maximize the potential of graphene. Some researchers have previously adsorbed SnO_2 on graphene to form a SnO_2-graphene composite with increased photovoltaic performance [7]. Cheng et al. improved the catalytic characteristics of graphene by catalytically producing TiO_2-graphene nanocomposites [8]. Our group decorated graphene with CdSe to form CdSe-rGo to study the structure and optical properties.

Over the last two decades, semiconductor nanoparticles have attracted considerable interest as being a major multidisciplinary field of study. From physics point of view, they are considered as a model system for understanding the transition from molecular to bulk-like material characteristics [9]. Due to their unique photophysical performance, semiconductor quantum dots (QDs) have been linked to a wide range of applications [10–14]., including quantum lasers, solar cells, light-emitting diodes, and bio-labeling, are among the various QDs [15–17]. Consequently, researcher have decorated CdSe on graphene sheets and examined the features of this unique nanocomposite. Chen et al. synthesized CdSe-rGO nanocomposite from graphene oxide and discovered that the nanocomposite showed high light absorption [18]. Nyoni et al. created

* Corresponding author at: Physics Department, Faculty of Science, Benha University, Benha 13518, Egypt.
E-mail address: tarek.attia@fsc.bu.edu.eg (T.S. Soliman).
[1] The first and second authors are equally contributed in this work.

https://doi.org/10.1016/j.jallcom.2021.162946
0925-8388/

CdSe-rGO nanocomposite as well investigated their electrical characteristics [19]. The nonlinear absorption characteristics of oxygen-containing defects in CdS-graphene were investigated by Zhu et al. [20]. Many researchers have investigated and made significant progress on the characteristics of CdSe-rGO composites. However, improving the distribution of CdSe on rGO in the composites should enhance the attributes of these CdSe-rGO compounds [21].

The Optical properties (optical band gap and refractive index) are the key factors to evaluate the material suitability as a suitable candidate for the optoelectronic applications [22–26]. These properties may be improved by manipulating CdSe nanoparticles sizes, in addition to the excellent distribution on the surface of graphene sheets [27]. The incorporation of CdSe nanoparticles onto graphene sheets improves its optical characteristics. CdSe-rGO nanocomposite possesses excellent optical characteristics as the electrons of CdSe QDs in the nanocomposite are quickly transported to the graphene sheets, which increase the conduction rate between electrons and improve the optical characteristics of CdSe QDs [27,28].

The main goal of this paper is to analyze the effect of graphene sheets on the structure and optical characteristics of CdSe nanoparticles. Several samples were collected at different times during the preparations process based on the hot injection method to obtain different sizes. The effect of change in the particle size of the sample on the structure and optical parameters has been studied using XRD, UV-Vis, and TEM techniques.

2. Experimental work

2.1. Materials

All chemicals were used without any further purification. Cadmium oxide (Fluka, 99.99%), Graphite powder (Merck, 99.9995%), Selenium powder (Se) (Strem, 99%), Trioctylphosphine oxide (TOPO) (Fluka, 97%), Oleylamine (Sigma Aldrich, 70%), Trioctylphosphine (TOP) (Sigma Aldrich, 90%), Oleic Acid (Merck, 99%).

2.2. Synthesis of CdSe -rGO NPs

CdSe-rGO nanocomposite was synthesized based on the hot injection method that was published by Awad et al. [28]. The CdO powder (0.3 gm) was dissolved in Oleic acid (1.2 ml) followed by the addition of a mixture of 2 ml Oleyl amine and 2.0 g TOPO into the reaction container with continuous stirring and heating on a hotplate/stirrer. When the temperature rises to 200 °C, inject a pre-dissolved solution of 0.12 gm Se powder and 0.01 gm of GO dissolved in 3 ml of TOP into the reaction container with keeping the continuous stirring. Collect samples at different times of (1, 3, 7, 10, and 15 min) and labeled as (a, b, c, d, and e) respectively. The CdSe-rGO nanocomposite is separated from the supernatant by ultra-centrifugation then disperses the obtained precipitate in toluene (2 ml) and followed by the addition of methanol (5 ml) to coagulate the CdSe/rGO QDs then collect precipitate by ultra-centrifugation. Repeat this step several times to obtain pure CdSe/rGO NCs. Finally, the collected CdSe/rGO QDs are dispersed in hexane (5 ml), and then dried at 40 °C in a vacuum oven for 12 h, finally collected as powder. The chemical reaction is represented in Fig. 1.

2.3. Characterizations

The X-ray diffraction (XRD) of the CdSe and CdSe/rGO QDs samples were performed using a standard X′Pert Philips Materials Research diffractometer. The TEM and HR-TEM images of the CdSe/rGO QDs samples were performed using transmission electron microscope (Joel JEM-2100) operated at 200 kV. UV-Visible absorption spectra of the CdSe and CdSe/rGO samples were operated using a double beam spectrophotometer (Perkin Elmer Lambda 40). Photoluminescence spectra of the CdSe and CdSe/rGO samples were recorded using a PerkinElmer LS55 Spectrofluorometer equipped with a xenon short-arc lamp as an exciting source.

3. Results and discussion

3.1. XRD and TEM analysis

The phase purity and crystalline structure of the as-prepared CdSe-rGO nanocomposite were explored using X-ray diffraction. As shown in Fig. 2a.

The XRD patterns revealed four distinct peaks at 25°, 30°, 42°, and 50° correspond to the (111), (200), (220) and (311) planes respectively of the CdSe cubic phase with reference code (JCPDS-XRD Cards no: 04-004-1009). The GO in the CdSe/rGO nanocomposite should be reduced to rGO after performing the chemical reaction at 200°C in presence of the Oleyl amine which serves as a capping agent for the as-synthesized CdSe QDs, and a reducing agent for GO at the same time. However, the low percentage of GO that leads to the formation of a low amount of rGO, causes the disappearance of the diffraction peaks of rGO in the XRD pattern. Also, the sharp peak at (2θ = 10.8) which corresponds to the reflection plane of GO

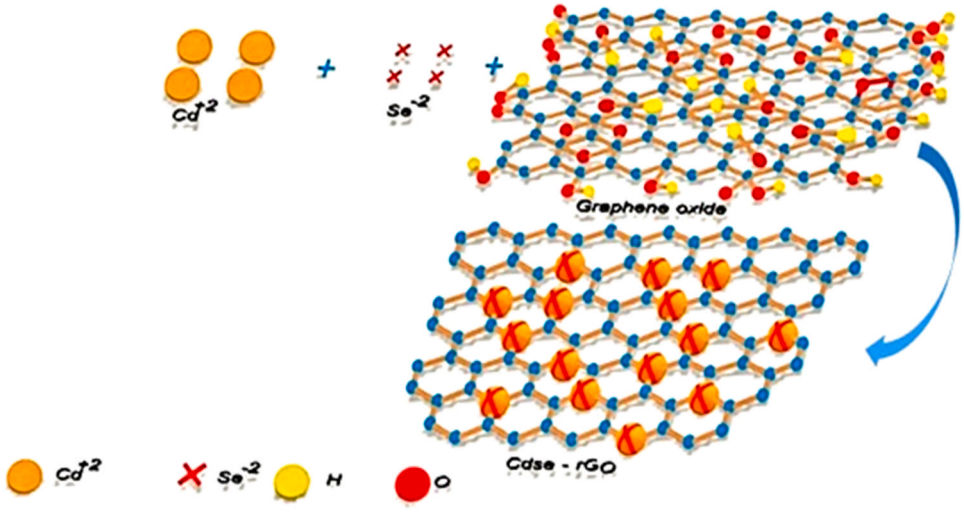

Fig. 1. Schematic representation of the synthesis of CdSe/rGO nanocomposites.

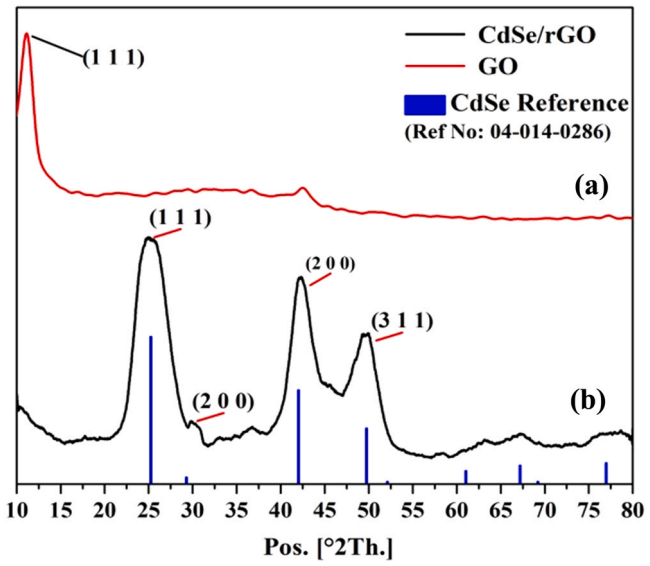

Fig. 2. Shows the XRD of (a) GO and (b) CdSe-rGO.

disappeared in the XRD pattern of the CdSe-rGO nanocomposite which indicates the reduction of GO into rGO see Fig. 2. b. The average particle size (L) of the supported CdSe QDs on graphene sheets was calculated using Debye–Scherrer's formula [L = 0.89 λ/w cos(θ)], where λ is the X-ray wavelength, w is the full-width at half-maximum and θ is the scattering angle [29,30]. The estimated particle size L for sample b, from the XRD humps for the as-synthesized CdSe on graphene sheet sample was about 3.43 nm which can be seen in Table 1.

Fig. 3(a) shows the TEM images of the GO nanosheets which are characterized by wrinkling their sheets, these wrinkles are responsible for the stability of the GO as well as the rGO because they prevent the Go or rGO layers from restacking again after the exfoliation process [31]. Fig. 3(b, d, and e) show the TEM images of the CdSe-rGO nanocomposite for samples b (at 3 min) and sample e (at 15 min) respectively. It reveals the edges and the wrinkles of the rGO which indicates the presence of the rGO in the as-prepared composite. In addition that the CdSe QDs are well distributed on the surface of the rGO layers as well as they are tightly anchored to the rGO surface, which enhance the electrical conductivity, monodispersity, and decreasing the surface traps and dangling bonds of the CdSe QDs [28]. The HR-TEM in Fig. 3(c, f), for the CdSe-rGO nanocomposite of the samples number (b) and (e) respectively, show the monodisperse and the uniform shape of the CdSe QDs. It has an average size of about 3 nm and 5 nm, respectively. The particle sizes data summarized in Table 1. Fig. 3(g, h) show CdSe QDs are monodispersed with uniform shape and average particle size approximately 4 nm (at 3 min) with relatively good morphology and largest particle size of 6.8 nm (at 15 min).

The size of nanoparticles was calculated from the peak maxima of the absorption spectra using two methods. The first method is the Polynomial Fitting Functions (*PFF*) taken by [32]**:**

$$D = (1.6122 \times 10^{-9})\lambda^4 - (2.657 \times 10^{-6})\lambda^3 + (1.6242 \times 10^{-3})\lambda^2 - (0.4277)\lambda + (41.57)$$

Where D (nm) is the particle size of a given CdSe QDs in the CdSe-rGO nanocomposite and λ_{max} (nm) is the wavelength of the optical excitonic peak of the samples.

The second method used the effective mass approximation (EMA) model to calculate the particle size of the CdSe QDs in the CdSe-rGO nanocomposite [33–35].

$$E_{gn} = E_{gb} + \frac{h^2}{8R^2}\left[\frac{1}{m_e} + \frac{1}{m_h}\right] - \frac{1.8e^2}{4\pi\varepsilon\varepsilon_0 R} \quad (1)$$

Where E_{gb} (1.74 eV) is the bulk crystal bandgap value [36], E_{gn} is the nanocrystal bandgap value, R is the radius of the CdSe QDs, m_e is the electron effective mass (0.13 m_o), m_h is the hole effective mass (0.45 m_o) ($m_o = 9.11 \times 10^{-32}$ kg) and ε is the relative dielectric constant for CdSe QDs [37]**.** The average particle size of CdSe QDs in the CdSe-rGO nanocomposite is calculated using the values of E_{gn} derived from UV spectra in Eq. (1). As shown in Table 1, the particle sizes range from 4.64 nm for sample number (a) to 5.46 nm for sample number (e). As demonstrated in Table 1, the results obtained from TEM images are consistent with the XRD results, PPT (first method), and EMA (second method) calculated values.

3.2. FTIR analysis

FT-IR spectra of GO, CdSe, and CdSe-rGO are displayed in Fig. 4. The GO spectrum reveals various stretching vibration peaks of O-H, C═O (in –COOH), C═C, and alkoxy C-O at 3435 cm^{-1}, 1731 cm^{-1}, 1621 cm^{-1}, and 1063 cm^{-1}, respectively [27]. The CdSe-rGO spectrum show some peaks at 3435 cm^{-1}, 1731 cm^{-1}, 1621 cm^{-1}, and 1063 cm^{-1} which are corresponding to O-H, C═O, C═C, and alkoxy C-O of the rGO, respectively. These peaks aren't appeared in the spectrum of CdSe QDs, this confirm that the CdSe QDs are attached to the rGO sheets. The amine ($-NH_2$) functional group of oleyl amine would react with the hydroxyl and carboxyl functional groups in GO to form amide bonding or amide-like structure. In the end, the long-chain amino group was grafted on the basal plane of GO, and GO was reduced simultaneously. The intensity of O-H and C═O of the carboxylic group of the GO that appeared at 3435, 1731 cm^{-1} respectively are remarkably reduced, representing that most of the oxygen groups on the GO surface are reduced during the chemical reaction. This means that the hydroxyl and carboxylic groups on the surface of GO are reduced by the amine group of the Oleyl amine. In addition to the thermal effect which facilitates the reduction process. These approaches for reduction of GO are in good match with the literature [38–42].

Table 1
The energy gap and the calculated particle size from TEM, EMA, PPT, and X-Ray.

Samples	Energy gap *using Tauc's equation* (eV)	Energy gap *from the absorption measurements* $E_g = hc/\lambda$ (eV)	Particle size $_{EMA}$ using Tauc's equation (nm)	Particle size $_{EMA}$ *from the absorption measurements* (nm)	Particle size $_{ppt}$ (nm)	Particle size $_{TEM}$ (nm)	Particle size $_{X\text{-}RAY}$ (nm)
a	2.15	2.33	5.46	4.64	2.74	–	–
b	2.10	2.25	5.80	4.96	3.10	3	3.43
c	2.06	2.21	6.10	5.14	3.28	–	–
d	2.05	2.17	6.20	5.36	3.63	–	–
e	2.03	2.15	6.38	5.46	3.72	5	–

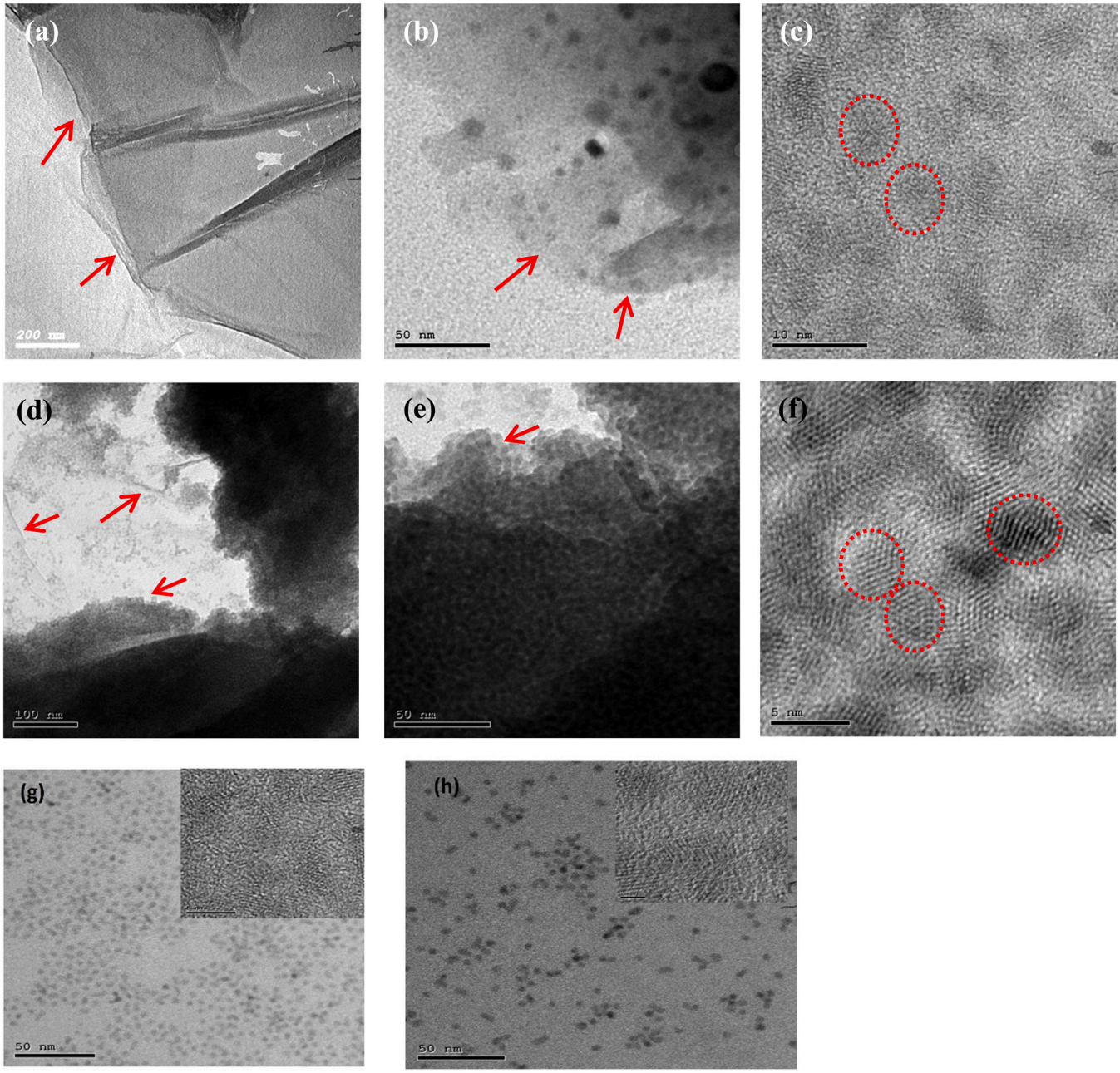

Fig. 3. TEM images of: (a) the as-prepared GO nanosheets via hummer method, (b, c) CdSe/rGO semiconductor nanocomposite (sample b, at 3 min), (d-f) CdSe/rGO semiconductor nanocomposite (sample e, at 15 min), and (g, h) CdSe QDs (3 min) and (15 min), respectively.

3.3. Optical properties

The absorption and emission spectra were measured for the CdSe QDs and CdSe-rGO nanocomposite. Fig. 5 shows the optical absorption spectra of CdSe QDs and the CdSe-rGO nanocomposite.

Fig. 5a shows a redshift in the wavelength as the reaction time increases, which indicates the grown of the particle size for CdSe QDs which is attributed to the quantum confinement effect [11,28]. The effect of rGO on CdSe QDs is shown on the absorption spectra in Fig. 5b. The absorption spectra of CdSe-rGO revealed that they are blue shifted with respect to the bare CdSe QDs. This confirms the lower particle size of CdSe-rGO than the CdSe QDs. It testifies that CdSe QDs are supported on rGO sheets. The rGO sheets decrease the rate of particle growth due to surrounding QDs with the rGO sheet, their growth rate will be lower than that of CdSe QDs. This leads to the formation of CdSe QDs crystals with lower defects (No surface traps), this is shown at the emission spectra of CdSe and CdSe-rGO, Fig. 6.

The full width at half maximum (FWHM) for the CdSe and CdSe-rGO QDs was calculated from their emission spectra. It's noticed from the emission spectra that CdSe-rGO QDs have narrower bands (small FWHM) than that of CdSe QDs; this indicates that the rGO enhances the particle growth with small size distribution. Stokes shift between the absorption and emission spectra for the CdSe-rGO sample is larger than that of CdSe QDs. This prove that the rGO increase the stokes shift of the CdSe QDS.

The observed absorption band for the CdSe QDs in the CdSe-rGO nanocomposite samples a, b, c, d, and e are at 533 nm (E_g= hc /λ = 2.33 eV), 551 nm (2.25 eV), 561 nm (2.21 eV), 574 nm (2.17 eV), and 577 nm (2.15 eV), respectively that can be seen in Table 1.

The peak maxima in the absorption spectra of CdSe QDs in the CdSe-rGO nanocomposite are shifted dramatically toward the visible

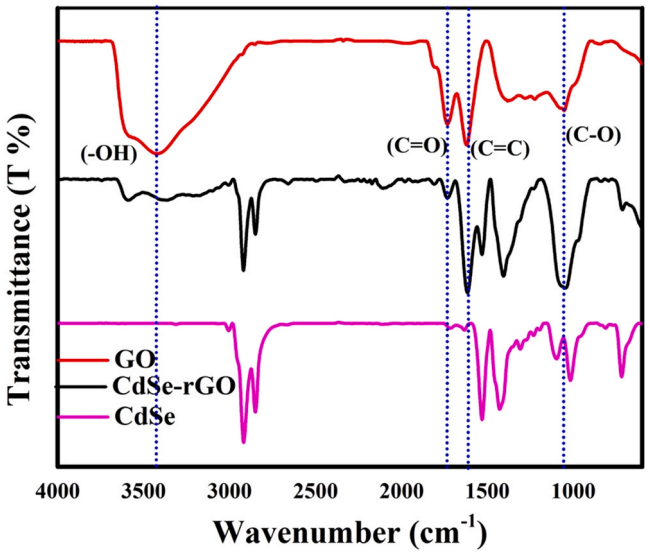

Fig. 4. FT-IR spectra of GO, CdSe, and CdSe-rGO.

region (red-shifted) that indicates increasing the particle size for CdSe QDs. Graphene not only has high electron mobility but also suppresses the recovery of electron holes. Therefore, the addition of Graphene causes a change in the electron transport mode and efficiency of CdSe QDs [27]. The red shift of absorbance of absorption spectra of composition to longer wavelength may be due to the changing quantum confinement effect [35] and mainly affecting by grapheme [27].

The transmission spectra of CdSe-rGO nanocomposite are shown in Fig. 7. It is clearly seen that the transmission decreases with an increase in the particle size for CdSe QDs in the surface of graphene sheet. This is owing to the agglomeration [28].

The electronic transitions are the essential parameter of the optical absorption. These transitions are controlled by certain selection rules, which can be expressed by using Tauc's equation [23,25,26],

$$\alpha h\upsilon = A\,(h\upsilon - E_g)^m \qquad (2)$$

where α is the absorption coefficient, $h\upsilon$ is the energy of the incident photons, A is a constant, and m is a constant with allowed values of (1/2 and 2), not allowed values of (3/2 and 3) for direct and indirect transitions, respectively [23,25,43]**.** The Tauc-plot curve of $(\alpha h\upsilon)^2$ value against $(h\upsilon)$ as seen in Fig. 8 determines the actual value of the band gap**.** The bandgap values of CdSe QDs in the CdSe-rGO nanocomposite were calculated from the energy axis's intercept by using the Tauc-plot computation. In Table 1, the bandgap values were retrieved.

As shown in Fig. 8 and Table 1, the optical bandgap increases as the size of the CdSe QDs in the CdSe-rGO nanocomposite decreases and vice versa. In other words, as particle size increases, the absorption edge shifts towards lower bandgap values, from 2.15 eV (5.46 nm) to 2.03 eV. (6.38 nm). This is related to the influence of quantum confinement effect. As it is established that the bandgap decreases upon increasing the nanoparticle size which is related to

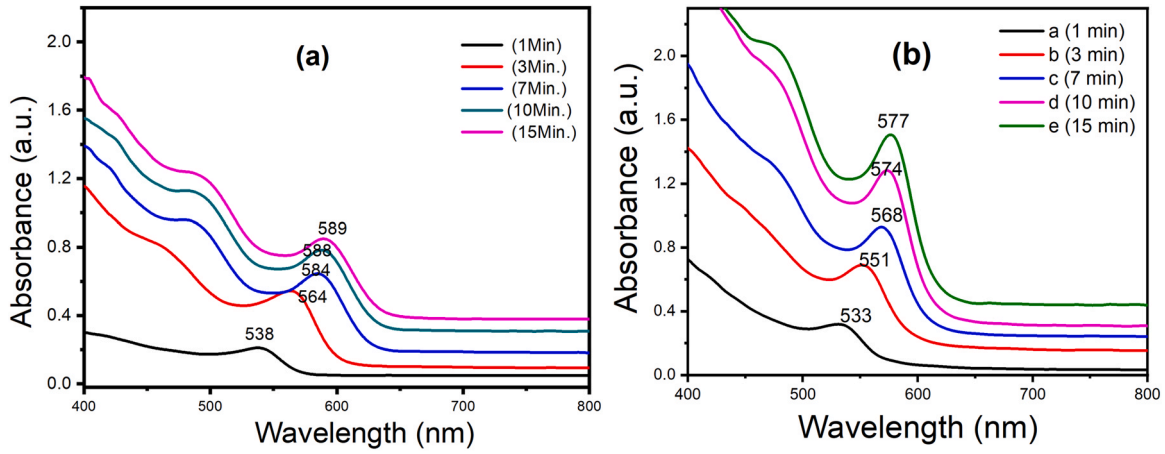

Fig. 5. The absorption spectra of; (a) CdSe QDs and (b) CdSe-rGO at different reaction time.

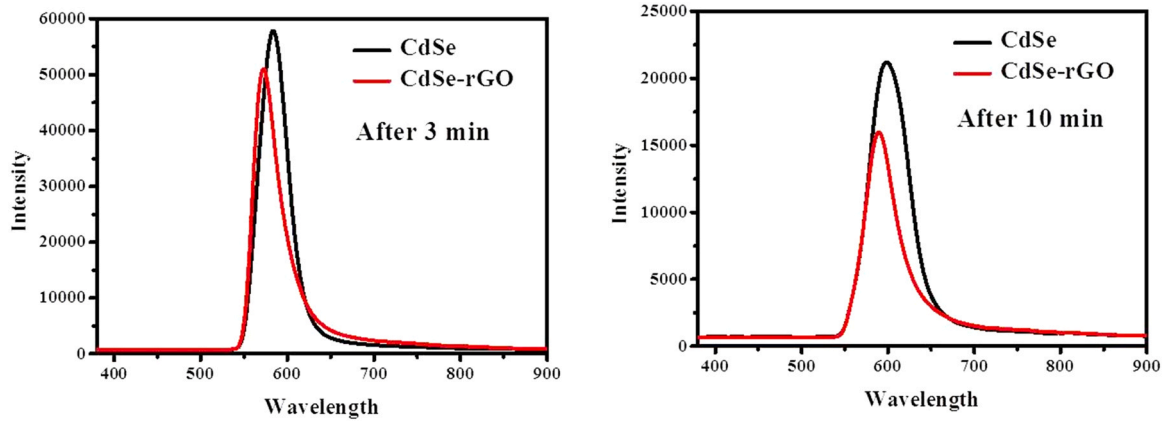

Fig. 6. The emission spectra of CdSe and CdSe-rGO at different reaction time.

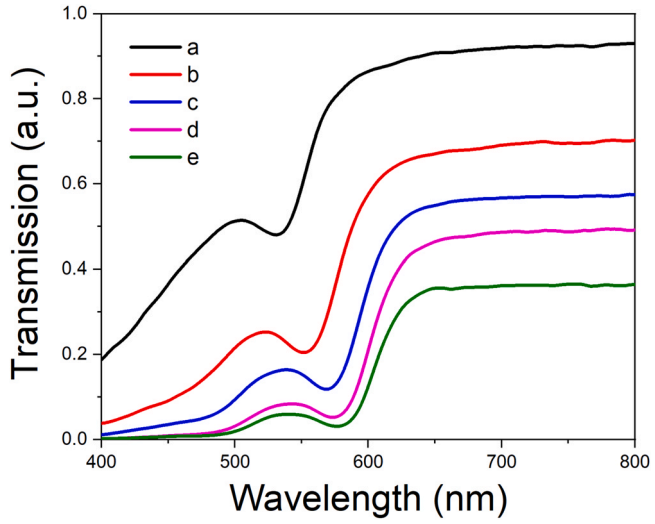

Fig. 7. The transmission vs. the wavelength for different samples of CdSe-rGO nanocomposite.

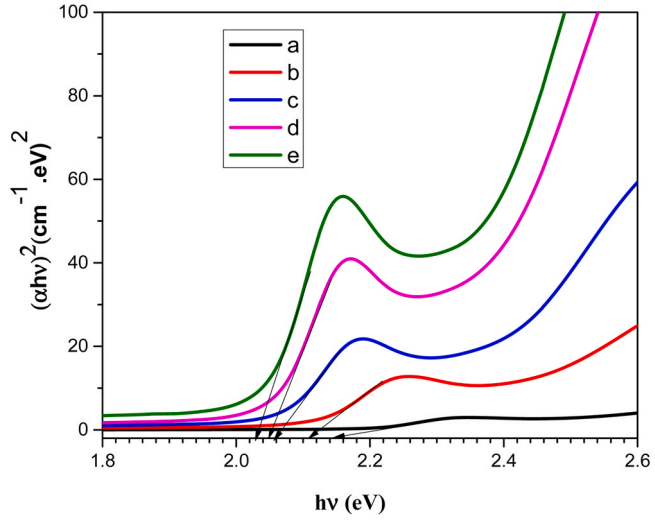

Fig. 8. $(\alpha h\upsilon)^2$ was plotted vs $(h\upsilon)$ for synthesized CdSe -rGO NPs samples.

the quantum confinement effect [26,43]. Hence, the bandgap of such materials can be tunable for appropriate opto-electronic applications.

3.4. Refractive index and extinction coefficient

The refractive index (n) and extinction coefficient (k) are significant optical parameters that play a key role in optical device design. The following equation is being used to compute these parameters [23,25,26];

$$\boldsymbol{n} = \left[\frac{\mathbf{1}+\boldsymbol{R}}{\mathbf{1}-\boldsymbol{R}}\right] + \sqrt{\left[\frac{\mathbf{4}\boldsymbol{R}}{(\mathbf{1}-\boldsymbol{R})^2}\right] - \boldsymbol{k}^2} \quad (3)$$

$$\boldsymbol{k} = \frac{\alpha\lambda}{\mathbf{4}\pi} \quad (4)$$

where R is the reflectance, [R = 1-(T * e^A)$^{1/2}$], T is the transmission, and A is the absorption. The variations of n and k with the wavelength of the incident light for different particle sizes of CdSe QDs in the CdSe-rGO nanocomposite are seen in Fig. 9.

As the wavelength increases, the refractive index decreases until it reaches its maximum value related to the CdSe particles, then reduces followed by plateau region from 625 nm to 800 nm (n practically constant), as illustrated in Fig. 9a. This maximum point red shifted with the increase of the particle size of CdSe in the CdSe-rGO nanocomposite. In the strong absorption region, an increase in the refractive index may be due to the incident wavelength coincident with the plasma frequency, whereas a decrease in the refractive index is attributed to normal dispersion of light with decreased absorption and increased transmittance [26,45–47]. Furthermore, as the particle size increases, the material transparency decreases, and its reflectivity increases consequently. Also, the low value of the refractive index, at lower particle size, indicates low packing density. Whilst, as the particle size increases, the packing density of the particles rose, and the refractive index increases as well [28,44].

The variance of the extinction coefficient as a function of wavelength for different sizes of CdSe QDs in CdSe-rGO nanocomposite can be seen in the Fig. 9b. The k plot exhibits the same behavior as the refractive index plot, except that after the maximum point, it declines slowly and practically constant at wavelength > 600 nm. Furthermore, the k values for sample (e) are larger than those for samples (d, c, b, and a). This indicates an increase in the amount of

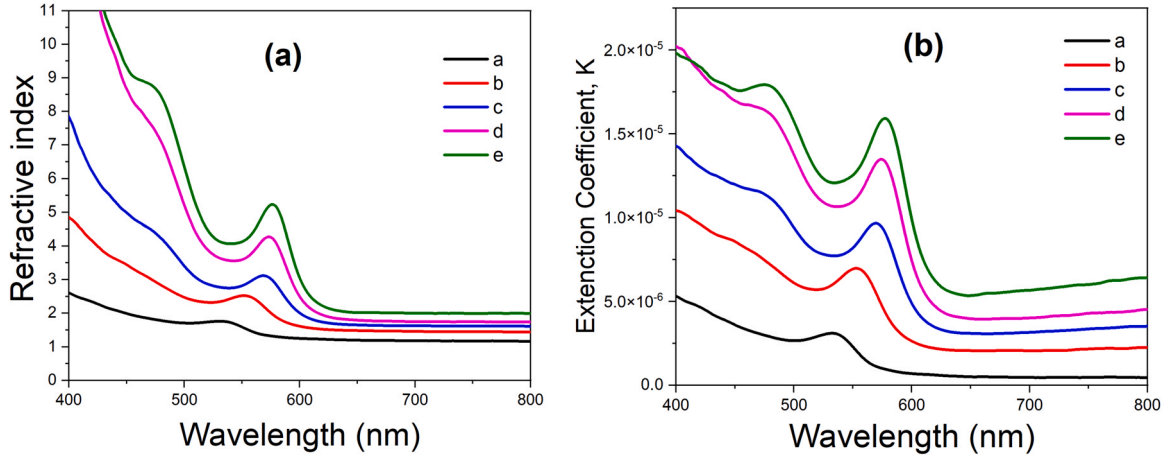

Fig. 9. (a) Refractive index and (b) Extinction coefficient as a function of wavelength for different sizes of CdSe QDs in the CdSe-rGO nanocomposite.

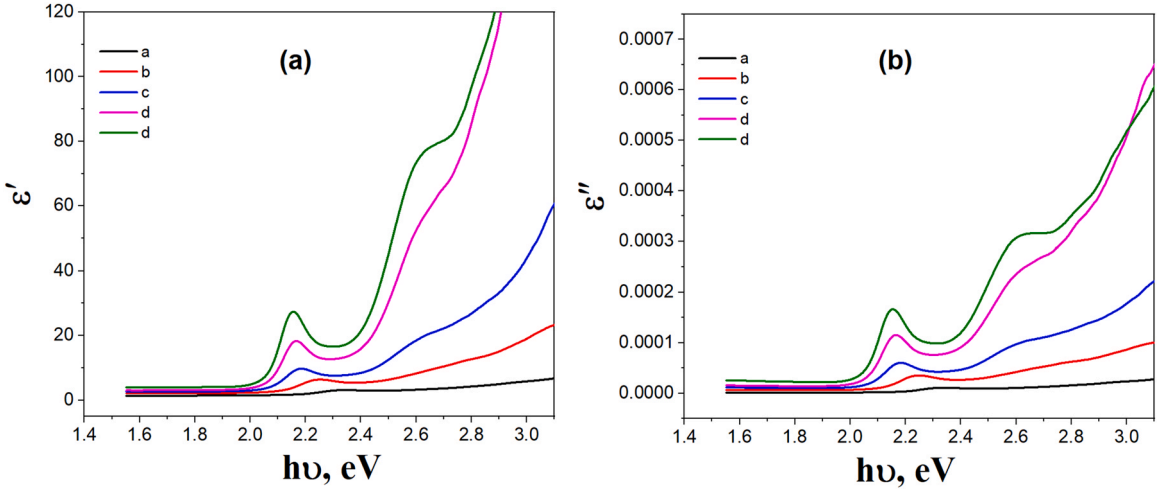

Fig. 10. Variation of (a) ε′ and (b) ε″ as a function of photon energy for different sizes of CdSe QDs in the CdSe-rGO nanocomposite.

energy lost from the material due to absorption, and the bigger particle size.

3.5. Optical dielectric parameters and optical conductivity

The optical dielectric properties are connected to the energy density of states from inside optical bandgap of the samples and reflect on the band structure of the material. The optical dielectric constant (ε′) represents the value of the increasing speed of light in the material, whereas the optical dielectric loss (ε″) represents the energy absorption by an electric field due to dipole motions in materials. The ε′ and ε″ can be calculated from the refractive index and extinction coefficient data using the following relations [25,44,47].

$$\varepsilon' = n^2 - k^2 \quad (5)$$

$$\varepsilon'' = 2nk \quad (6)$$

Fig. 10 shows the relation between the optical dielectric characteristic and the photon energy for different sizes of CdSe QDs in the CdSe-rGO nanocomposite.

It is obvious that ε′ and ε″ values have a maximum in the range from 2.1 eV to 2.3 eV. This in coincided with the maximum absorption of CdSe QDs in the CdSe-rGO nanocomposite. Moreover, these values increase as the particle size of the CdSe QDs increases.

The optical conductivity $\sigma_{opt.}$ is connected with the optical band gap of the materials, and it was dependent on many parameters as shown in the following relation [25,26].

$$\sigma_{opt.} = \alpha\, n\, c/4\pi \quad (7)$$

where c is the speed of light. The relation between the optical conductivity versus the photon energy of CdSe QDs in the CdSe-rGO nanocomposite is shown in Fig. 11.

It is observed that optical conductivity increased as particle size of the CdSe QDs in the CdSe-rGO nanocomposite increase.The presence of more CdSe QD nanoparticles in the CdSe-rGO nanocomposite enhances the density of localized states in the band structure, causing the absorption coefficient and optical conductivity to increase [26,44]. At the lower photon energy ($1.6 < h\upsilon < 2$ eV), the optical conductivity almost constant. While at $h\upsilon > 2.1$ eV, the optical conductivity increases. This is connected to the development of localized tail states in the forbidden bandgap, which functions as a transition point, assisting in electron transfer from the valence band to the tail and to the conduction band [23,26]. These localized states

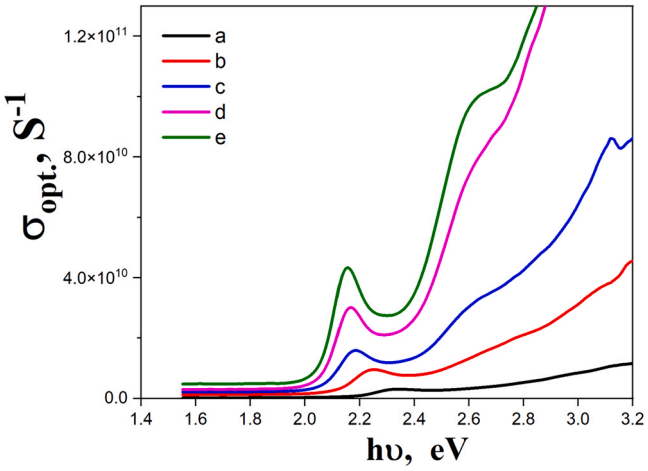

Fig. 11. The variation of the optical conductivity versus the photon energy for different sizes of CdSe QDs in the CdSe-rGO nanocomposite.

lead to a decrease in the bandgap and an increase in the optical conductivity as well. In addition, the free charge carriers are produced from the excited electrons by photon energy and high absorbance of CdSe-rGO nanocomposite [26,47].

3.6. Skin depth

Skin depth and the optical conductivity are important parameters associated with the absorption of photons by nanoparticles. The photon density decreases exponentially from the material surface to inside it owing to different parameters like refractive index, surface morphology, and material density. The skin depth (δ) can be calculated using the inverse of the absorption coefficient [26].

$$\delta = 1/\alpha \quad (8)$$

Fig. 12 shows the variation of skin depth as a function of photon energy for CdSe QDs in the CdSe-rGO nanocomposite. It is observed that δ decreases as photon energy increase up to cut off wavelength λ_{cutoff} ~ 2.5 eV, and then increases exponentially for CdSe QDs in the CdSe-rGO nanocomposite. Moreover, the skin depth decreases as the size of CdSe QDs increases.

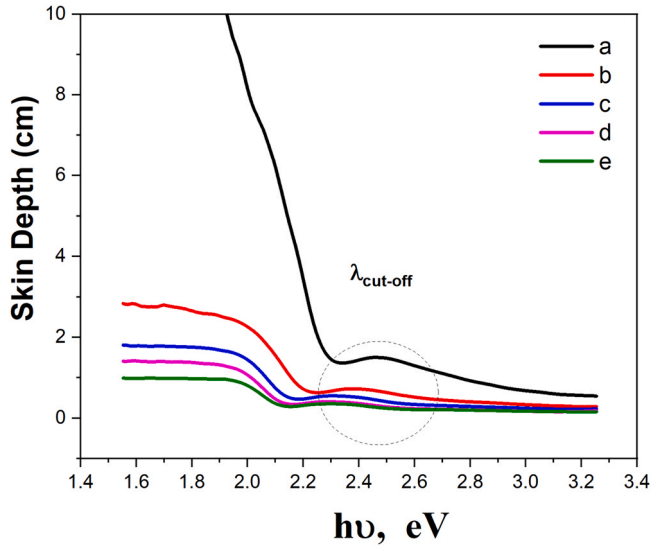

Fig. 12. The skin depth versus the photon energy of CdSe QDs in the CdSe-rGO nanocomposite.

4. Conclusion

Five samples of CdSe-rGO nanocomposite with different particle sizes of CdSe QDs were synthesized by the hot injection method. The average particle size of samples and bandgap are calculated with different methods. TEM analysis has verified the consistency of the particle sizes obtained with those obtained by an EMA and PPT with those obtained from XRD data. The impact of particle sizes on the optical parameters was investigated using UV–visible absorption spectra. It was found that direct optical bandgap, refractive index, extinction coefficient, optical dielectric, and optical conductivity increases have been significantly influenced by the change of the particle size of the CdSe QDs in the CdSe-rGO nanocomposite. The obtained CdSe-rGO nanocomposite in this work provides an opportunity for tuning the optical parameters by controlling their particle sizes to achieve better performance of device fabrication.

CRediT authorship contribution statement

Ahmed I. Abdel-Salam: Investigation, Methodology, Formal analysis, Writing – review & editing. **M.M. Awad:** Investigation, Methodology, Formal analysis, Writing – review & editing. **T. S. Soliman:** Data curation, Formal analysis, Writing – review & editing. **A. Khalid:** Supervision, Conceptualization, Formal analysis, Investigation, Writing – review & editing.

Declaration of Competing Interest

The authors declare that they have no known competing financial interests or personal relationships that could have appeared to influence the work reported in this paper.

References

[1] K.S. Novoselov, V.I. Fal'ko, L. Colombo, P.R. Gellert, M.G. Schwab, K. Kim, A roadmap for graphene, Nature 490 (7419) (2012) 192–200.
[2] M. Zhao, Direct synthesis of graphene quantum dots with different fluorescence properties by oxidation of graphene oxide using nitric acid, Appl. Sci. 8 (8) (2018) 1303.
[3] P. Avouris, Graphene: electronic and photonic properties and devices, Nano Lett. 10 (11) (2010) 4285–4294.
[4] D. Chen, L. Tang, J. Li, Graphene-based materials in electrochemistry, Chem. Soc. Rev. 39 (8) (2010) 3157–3180.
[5] R. Maria-Hormigos, B. Jurado-Sánchez, A. Escarpa, Graphene quantum dot based micromotors: a size matter, Chem. Commun. 55 (47) (2019) 6795–6798.
[6] T. Tabish, S. Zhang, Graphene quantum dots: syntheses, properties and biological applications, Graphene Nanocomposites for Cancer Diagnosis and Regenerative Medicine, (2016).
[7] Q. Guo, Z. Zheng, H. Gao, J. Ma, X. Qin, SnO2/graphene composite as highly reversible anode materials for lithium ion batteries, J. Power Sources 240 (2013) 149–154.
[8] P. Cheng, Z. Yang, H. Wang, W. Cheng, M. Chen, W. Shangguan, G. Ding, TiO2–graphene nanocomposites for photocatalytic hydrogen production from splitting water, Int. J. Hydrog. Energy 37 (3) (2012) 2224–2230.
[9] Q.A. Darugar, Surface effects on the ultrafast electronic relaxation of some semiconductor and metallic nanoparticles, Georgia Institute of Technology, 2006.
[10] D. Patidar, et al., Energy band-gap and conductivity measurement of CdSe thin films, Chalcogenide Lett. 5 (2) (2008) 21–25.
[11] X. Liu, X. Ji, M. Liu, N. Liu, Z. Tao, Q. Dai, L. Wei, C. Li, X. Zhang, B. Wang, High-performance ge quantum dot decorated graphene/zinc-oxide heterostructure infrared photodetector, ACS Appl. Mater. Interfaces 7 (2015) 2452–2458, https://doi.org/10.1021/AM5072173
[12] A. De Martino, R. Egger, On the spectrum of a magnetic quantum dot in graphene, Semicond. Sci. Technol. 25 (2010) 034006, https://doi.org/10.1088/0268-1242/25/3/034006
[13] P. Guyot-Sionnest, Colloidal quantum dots, Comptes Rendus Phys. 9 (8) (2008) 777–787.
[14] A. Abdel-Salam, et al., Anisotropic CuInSe2 nanocrystals: synthesis, optical properties and their effect on photoelectric response of dye-sensitized solar cell, Rev. Mex. De Física 66 (1) (2020) 14–22.
[15] Jr Bruchez M, M. Moronne, P. Gin, S. Weiss, A.P. Alivisatos, Semiconductor nanocrystals as fluorescent biological labels, Science 281 (5385) (1998) 2013–2016.
[16] H. Lee, J. Lim, J. Song, H. Heo, K. An, J. Kim, S. Lee, K. Char, H.J. Song, C. Lee, CdSe tetrapod interfacial layer for improving electron extraction in planar heterojunction perovskite solar cells, Nanotechnology 30 (6) (2018) 065401.
[17] V.I. Klimov, A.A. Mikhailovsky, S. Xu, A. Malko, J.A. Hollingsworth, C.A. Leatherdale, H. Eisler, M.G. Bawendi, Optical gain and stimulated emission in nanocrystal quantum dots, Science 290 (5490) (2000) 314–317.
[18] W.C. OH, M. CHEN, K. CHO, C. KIM, Z. MENG, L. ZHU, Synthesis of graphene-CdSe composite by a simple hydrothermal method and its photocatalytic degradation of organic dyes, Chin. J. Catal. 32 (9–10) (2011) 1577–1583.
[19] S. Nyoni, T. Nyokong, Development of graphene/CdSe quantum dots-co phthalocyanine nanocomposite for oxygen reduction reaction, Electroanalysis 26 (10) (2014) 2261–2272.
[20] B. Zhu, et al., Oxygen-containing-defect-induced synergistic nonlinear optical enhancement of graphene/CdS nanohybrids under single pulse laser irradiation, Photon. Res. 6 (12) (2018) 1158–1169.
[21] L.L. Beecroft, C.K. Ober, Nanocomposite materials for optical applications, Chem. Mater. 9 (6) (1997) 1302–1317.
[22] A.L. Stepanov, Optical Properties of Polymer Nanocomposites with Functionalized Nanoparticles, in Polymer Composites with Functionalized Nanoparticles, Elsevier, 2019, pp. 325–355.
[23] T. Soliman, S. Vshivkov, Effect of Fe nanoparticles on the structure and optical properties of polyvinyl alcohol nanocomposite films, J. Non-Cryst. Solids 519 (2019) 119452.
[24] K. Waszkowska, O. Krupka, O. Kharchenko, V. Figà, V. Smokal, N. Kutsevol, B. Sahraoui, Influence of ZnO nanoparticles on nonlinear optical properties, Appl. Nanosci. 10 (12) (2020) 4977–4982.
[25] T. Soliman, S. Vshivkov, S.I. Elkalashy, Structural, linear and nonlinear optical properties of Ni nanoparticles–polyvinyl alcohol nanocomposite films for optoelectronic applications, Opt. Mater. 107 (2020) 110037.
[26] A.S. Hassanien, A.A. Akl, Influence of composition on optical and dispersion parameters of thermally evaporated non-crystalline Cd50S50-xSex thin films, J. Alloy. Compd. 648 (2015) 280–290.
[27] P. Li, B. Zhu, P. Li, Z. Zhang, L. Li, Y. Gu, A facile method to synthesize CdSe-reduced graphene oxide composite with good dispersion and high nonlinear optical properties, Nanomaterials 9 (7) (2019) 957.
[28] M.M. Awad, A.I. Abdel-Salam, S.A. Elfeky, H.S. Rady, A.S. Hassanien, M.B. Mohamed, Y.H. Elbashar, Tuning the optical properties of CdSe quantum dot using graphene nanocomposite, J. Opt. 48 (4) (2019) 616–625.
[29] M. Pattabi, S.A. B, Effect of precursor concentration on the particle size of mercaptopropionic acid-capped CdS nanoparticles, J. N. Mater. Electrochem. Syst. 10 (1) (2007) 43–47.
[30] V.L. Calero-DdelC, C. Rinaldi, Synthesis and magnetic characterization of cobalt-substituted ferrite (CoxFe3-xO4) nanoparticles, J. Magn. Magn. Mater. 314 (1) (2007) 60–67.
[31] J.C. Meyer, A.K. Geim, M.I. Katsnelson, K.S. Novoselov, T.J. Booth, S. Roth, The structure of suspended graphene sheets, Nature 446 (7131) (2007) 60–63.
[32] X.M. Shao, J.Z. Lin, Z.S. Yu, Experimental determination of the extinction coefficient of CdTe, CdSe, and CdS nanocrystals, Chem. Mater. 15 (14) (2003) 2854–2860.
[33] O. Madelung, Semiconductors—Basic Data, Springer Science & Business Media, 2012.
[34] R. Sathyamoorthy, P. Sudhagar, R.S. Kumar, T.M. Sathyadevan, Low temperature synthesis of thiol-functionalized CdTe nanoclusters with different tellurium contents, Cryst. Res. Technol. J. Exp. Ind. Crystallogr. 45 (1) (2010) 99–103.

[35] C.P. Shah, M. Rath, M. Kumar, P.N. Bajaj, Precursor concentration and temperature controlled formation of polyvinyl alcohol-capped CdSe-quantum dots, Beilstein J. Nanotechnol. 1 (2010) 119–127.
[36] J.-H. Yum, S.H. Choi, S.S. Kim, D.Y. Kim, Y.E. Sung, CdSe quantum dots sensitized TiO 2 electrodes for photovoltaic cells, J. Korean Electrochem. Soc. 10 (4) (2007) 257–261.
[37] O. Madelung, Semiconductors: Data Handbook, Springer Science & Business Media, 2004.
[38] R.V. Digraskar, V.S. Sapner, A.V. Ghule, B.R. Sathe, Enhanced overall water-splitting performance: oleylamine-functionalized go/cu2znsns4 composite as a nobel metal-free and nonprecious electrocatalyst, ACS Omega 4 (21) (2019) 18969–18977.
[39] Z. Liu, S. Niu, N. Wang, Oleylamine-functionalized graphene oxide as an electron block layer towards high-performance and photostable fullerene-free polymer solar cells, Nanoscale 9 (42) (2017) 16293–16304.
[40] Z. Tang, Z. Zhang, Z. Han, S. Shen, J. Li, J. Yang, One-step synthesis of hydrophobic-reduced graphene oxide and its oil/water separation performance, J. Mater. Sci. 51 (19) (2016) 8791–8798.
[41] W. Chen, L. Yan, P.R. Bangal, Preparation of graphene by the rapid and mild thermal reduction of graphene oxide induced by microwaves, Carbon 48 (4) (2010) 1146–1152.
[42] B. Zhao, P. Liu, Y. Jiang, D. Pan, H. Tao, J. Song, T. Fang, W. Xu, Supercapacitor performances of thermally reduced graphene oxide, J. Power Sour. 198 (2012) 423–427.
[43] F.G. Hone, et al., Synthesis and characterization of CdSe nanocrystalline thin film by chemical bath deposition technique, Int. J. Thin Fil. Sci. Technol. 4 (2) (2015) 69–74.
[44] T. Soliman, A. Abouhaswa, Synthesis and structural of Cd0.5Zn0.5 F2O4 nanoparticles and its influence on the structure and optical properties of polyvinyl alcohol films, J. Mater. Sci. Mater. Electron. 31 (12) (2020) 9666–9674.
[45] S. Yasmeen, F. Iqbal, T. Munawar, M.A. Nawaz, M. Asghar, A. Hussain, Synthesis, structural and optical analysis of surfactant assisted ZnO–NiO nanocomposites prepared by homogeneous precipitation method, Ceram. Int. 45 (14) (2019) 17859–17873.
[46] M. Shkir, M. Arif, V. Ganesh, A. Singh, H. Algarni, I.S. Yahia, S. AlFaify, An effect of Fe on physical properties of nanostructured NiO thin films for nonlinear optoelectronic applications, Appl. Phys. A 126 (2) (2020) 1–14.
[47] K. Sharma, A.S. Al-Kabbi, G.S.S. Saini, S.K. Tripathi, Determination of dispersive optical constants of nanocrystalline CdSe (nc-CdSe) thin films, Mater. Res. Bull. 47 (6) (2012) 1400–1406.